ESR and ENDOR Studies of Hippuric Acid Single Crystals X-Irradiated at 295 K: A Reinvestigation

Nimir Ali Salih,[†,§] Audun Sanderud,[†] Einar Sagstuen,*[,†] Omer I. Eid,[‡,§] and Anders Lund[‡]

Department of Physics, University of Oslo, P.O. Box 1048 Blindern, N-0316 Oslo, Norway, and Department of Physics and Measurement Technology, University of Linköping, S-581 83 Linköping, Sweden

Received: June 2, 1997; In Final Form: August 13, 1997[⊗]

Single crystals of the amino acid analogue hippuric acid, $PhCONHCH_2COOH$, have been X-irradiated at 295 K and studied using X-band EPR, ENDOR, and ENDOR-induced EPR (EIE) spectroscopy at 295 and 130 K. Two different radical species were observed and characterized. The dominant species is radical **R1**, $PhCONH\text{-}^{\bullet}CH_2$, supposedly formed by net decarboxylation from a pristine oxidation product. The nitrogen hyperfine and quadrupolar interactions yield information on the electronic structure in the nitrogen valence orbitals. The second radical species, radical **R2**, is formed by a net hydrogen addition to the phenyl entity of hippuric acid. As a reduction product, it may be formed by protonation of the negatively charged anion of the phenyl group, but the alternative mechanism of direct hydrogen addition to the phenyl ring cannot be ruled out. Spectral simulations indicate that radical **R1** contributes about 85% of the total EPR spectrum, while the remaining 15% is contributed by radical **R2**.

1. Introduction

ESR and ENDOR techniques have been extensively used in the study of radiation damage to the amino acids and their derivatives by ionizing radiation.[1,2] In most of the work the main objective has been to study the effect of radiation on the biologically important peptide linkage (−CO−NH−) which joins amino acids together into polyamino acids and proteins.[3,4] Hippuric acid (see structure below) is a naturally occurring amino acid analogue. It is an *N*-benzoyl derivative of glycine and may be considered to be similar to *N*-acetylglycine but with the methyl group replaced with a phenyl group. From a radiation-chemical point of view it is of interest to investigate the effect of the aromatic phenyl substituent on the primary radiation processes involving the peptide bond.

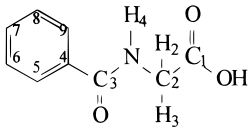

Previously, hippuric acid has been subject to two EPR and ENDOR studies. Votinov[5] reported the formation of a nitrogen-centered radical as a result of N−H bond rupture after γ-irradiation of polycrystalline hippuric acid. Chacko and co-workers[6] reported the formation of the *N*-benzoylamino methyl radical $R-^{\bullet}CH_2$ in a detailed ENDOR study of hippuric acid crystals X-irradiated at 295 K and measured at 77 K.

In the present work further details of the electronic structure of this radical are obtained, based on the analysis of nitrogen hyperfine and quadrupolar interaction. Furthermore, experimental evidence for one additional radical species, formed by a net hydrogen addition to the phenyl moiety, is presented. Mechanisms for the formation of the proposed radicals are discussed in light of the present knowledge of the radiation chemistry of amino acids and dipeptides.

2. Experiment

Hippuric acid single crystals were grown from aqueous solutions by slow evaporation. Partially deuterated samples were prepared in a similar manner by repeated recrystallization using 99.8% D_2O. The crystal structure of hippuric acid has been determined using neutron diffraction methods.[7] The crystals are orthorhombic with space group $P2_12_12_1$. The crystals were irradiated using 60 kV, 50 mA X-rays to doses in the 10−50 kGy range. The irradiated crystals were mounted to a goniometer head of a Weissenberg camera, and the rotation axes were aligned parallel to the respective crystallographic axes to within 0.5°. The crystals were then transferred to quartz crystal holders used for EPR and ENDOR measurements without loss of alignment. The irradiation caused the appearance of a pink coloration of the crystals, the intensity of which increased with the irradiation dose.

The X-band EPR, ENDOR, and EIE (ENDOR-induced EPR) measurements were carried out at 130 and 295 K using a Bruker ER 200D-SRC spectrometer as previously described.[8,9] The ENDOR data were analyzed using computer programs described.[9−11] Second-order corrections of the hyperfine couplings were not made. Spectral simulations were performed using a program described recently.[12]

3. Experimental Results and Analysis

Generally, the EPR spectra obtained after irradiation are dominated by an anisotropic 1:2:1 triplet, indicating interaction with two nearly equivalent protons. This is demonstrated in Figure 1, which shows EPR spectra obtained at 295 K from a partially deuterated crystal with the magnetic field along the crystallographic *a*-axis (Figure 1a) and the crystallographic *b*-axis (Figure 1b). Poorly resolved superhyperfine structure, indicating weaker hyperfine interactions, is observed at almost all orientations. Broader features on each wing of the spectra evidence the presence of a resonance due to one radical in addition to that giving rise to the main triplet.

* To whom all correspondence should be addressed.
[†] University of Oslo.
[‡] University of Linköping.
[§] Permanent address: Department of Physics, Faculty of Science, University of Khartoum, P.O. Box 321, Khartoum, Sudan.
[⊗] Abstract published in *Advance ACS Abstracts,* October 1, 1997.

S1089-5639(97)01788-X CCC: $14.00

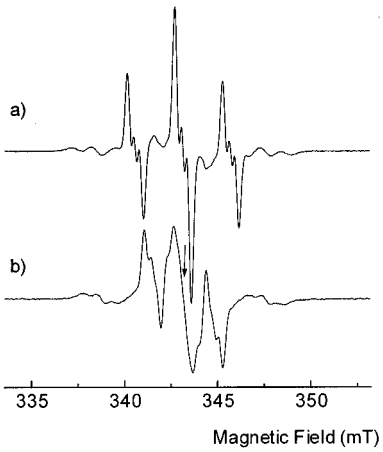

Figure 1. First-derivative EPR spectra from an X-irradiated single crystal of partially deuterated hippuric acid recorded at 295 K. In part a the external magnetic field is along ⟨*a*⟩; in part b it is along ⟨*b*⟩. The center of each spectrum is at $g = 2.0023$.

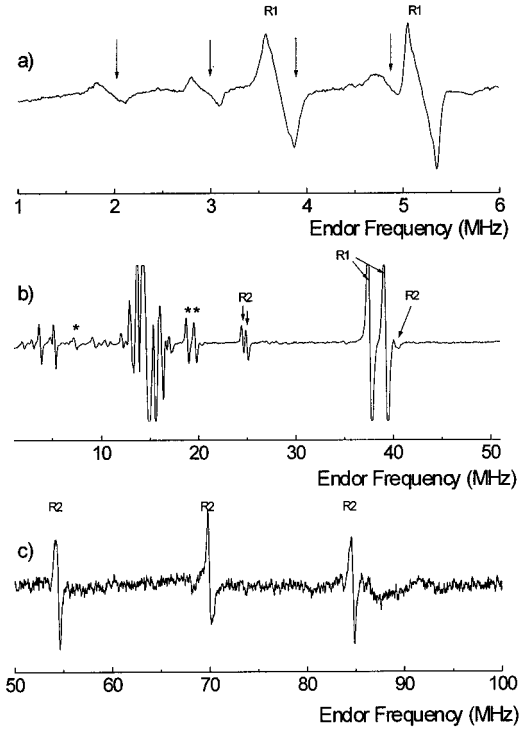

Figure 2. ENDOR spectra observed from an X-irradiated single crystal of hippuric acid at 295 K. The external magnetic field is parallel with ⟨*b*⟩. (a) 1−6 MHz rf-frequency sweep. The arrows indicate the lines assigned to the four ^{14}N resonance lines of radical **R1**. (b) 1−51 MHz rf-frequency sweep. Resonance lines due to the different radicals discussed in the text are marked. Lines marked with ∗ are instrumental artifacts due to nonlinearities of the rf-power amplifier. (c) 50−100 MHz rf-frequency sweep. Resonance lines due to the different radicals discussed in the text are marked.

ENDOR measurements were performed at 295 and 130 K. The ENDOR spectra obtained revealed altogether seven hyperfine interactions, which easily could be followed through all three planes of observation, one of these clearly being due to a weak interaction with ^{14}N. In the vicinity of the free proton frequency several resonance lines were observed but were not analyzed in the present work. Some of these interactions were discussed in the previous work[6] and shown mainly to be due to weak couplings to the protons in the phenyl ring of the *N*-benzoylamino methyl radical (**R1**, see below). Figure 2a shows a room-temperature ENDOR spectrum obtained by sweeping the rf frequency between 1 and 6 MHz, with the magnetic field locked to a position marked with an arrow in Figure 1b. Arrows denote the resonance lines assigned to a ^{14}N interaction. The two most intense lines in this spectrum are the low-frequency branches of two proton couplings from radical **R1**, to be discussed below. Figure 2b shows the corresponding ENDOR spectrum obtained while sweeping the rf frequency between 1 and 51 MHz, whereas Figure 2c shows the spectrum obtained by sweeping between 50 and 100 MHz. R1 and R2 indicate the lines assigned to the different radicals discussed below. It should be noted that lines marked with ∗ are second-harmonics of the strongest ENDOR lines due to nonlinearity of the rf-power amplifier. For all couplings two magnetically inequivalent sites were observed, in accord with the orthorhombic symmetry of the crystal.[7] The ENDOR-induced EPR (EIE) technique was used to assign the different ENDOR lines to specific EPR patterns, i.e. radicals. The two characteristic patterns obtained are shown in Figure 3. EIE was also used to confirm that the ^{14}N ENDOR resonance lines in Figure 2a are associated with the other resonance lines denoted by **R1** in Figure 2b. The hyperfine and quadrupolar coupling tensors deduced from the ENDOR data are given in Table 1 for radical **R1** and in Table 2 for radical **R2**. In particular, the data in Table 1 agree well with those derived from measurements at 77 K by Chacko and co-workers.

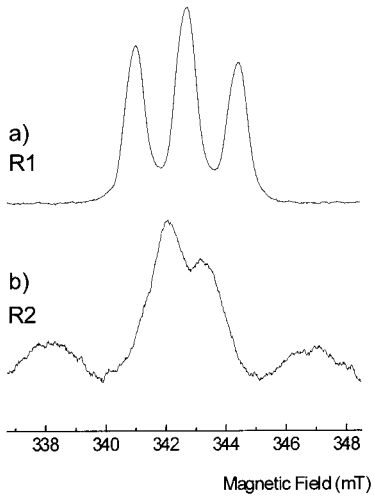

Figure 3. ENDOR-induced EPR spectra (EI-EPR or EIE) obtained from the ENDOR lines assigned to radical **R1** (a) and radical **R2** (b). The magnetic field sweep width was 11.8 mT in these experiments, and each spectrum is centered at $g = 2.0023$.

3.1. Radical R1: The *N*-Benzoylamino Methyl Radical. *3.1.1. Proton Interactions.* The dominant radical stabilized in the hippuric acid crystals yielding the triplet EPR pattern in Figure 1 is the *N*-benzoylamino methyl radical **R1**:

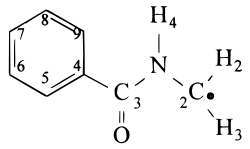

as previously shown by Chacko et al.[6] The two proton coupling tensors given in Table 1 are characterized by the large anisotropy typical of α-couplings, due to the strong dipolar interaction between the unpaired electron and the two methylene protons. EIE spectra (shown in Figure 3) clearly confirm the assignment of these ENDOR resonances, as well as those lines that are due to the ^{14}N interaction (Figure 2a), to the major triplet pattern of the EPR spectra.

The α-proton tensor data are similar to those previously published,[6] and the eigenvectors for the various principal values

TABLE 1: Hyperfine and Quadrupolar Coupling Tensors (MHz) for Radical R1 in Single Crystals of Hippuric Acid, X-Irradiated and Measured at 295 K. The Angle of Deviation between a Given Eigenvector and a Particular Reference Direction Is Given in Degrees[a]

			eigenvector			
tensor	isotropic value	principal values	⟨*a*⟩	⟨*b*⟩	⟨*c*⟩	angle of deviation[b]
$H_\alpha(1)$	−51.4(2)	−82.4(2)	0.861(2)	−0.470(4)	−0.192(6)	
		−50.5(3)	0.057(7)	−0.466(7)	0.883(4)	4.8[1], 7.3[c]
		−21.4(4)	0.504(3)	−0.750(4)	−0.428(8)	4.4[4]
$H_\alpha(2)$	−51.9(2)	−79.5(2)	0.896(2)	−0.353(4)	−0.269(6)	
		−49.8(2)	0.132(8)	−0.367(11)	0.921(4)	3.3[1], 7.3[c]
		−26.5(4)	0.424(4)	0.861(5)	0.283(12)	5.0[2]
^{14}N	−8.09(1)	−9.53(3)	−0.303(19)	0.864(5)	0.400(6)	43.3[2]
		−8.58(1)	0.951(6)	0.249(19)	0.181(8)	17.7[3]
		−6.16(2)	−0.057(8)	−0.436(4)	0.897(2)	8.6[1]
$Q(^{14}N)$	0.00	−0.846(6)	0.244(4)	−0.370(4)	0.896(2)	9.9[1]
		0.607(6)	0.967(1)	0.153(13)	−0.200(6)	10.1[3]
		0.238(5)	−0.063(14)	0.916(3)	0.396(5)	29.2[2]

[a] Uncertainties are given at the 95% confidence level in the last digit(s) of the quoted values. [b] Crystallographic directions:[7]

(1) ⊥ to C3−N−C2 fragment	0.0776	−0.3925	0.9164
(2) N−H4 bond direction	0.4329	0.8227	0.3685
(3) N−C2 bond direction	0.9963	0.0636	−0.0577
(4) N−C3 bond direction	0.5485	−0.7509	−0.3678

[c] Angle between the eigenvectors of the two intermediate α-proton coupling principal values.

TABLE 2: Hyperfine Coupling Tensors (MHz) for Radical R2 in Single Crystals of Hippuric Acid, X-Irradiated and Measured at 295 K. The Angle of Deviation between a Given Eigenvector and a Particular Reference Direction Is Given in Degrees[a]

			eigenvector			
tensor	isotropic value	principal values	⟨*a*⟩	⟨*b*⟩	⟨*c*⟩	angle of deviation[b]
H_α(C6)	−22.4(1)	−34.2(2)	−0.857(4)	−0.437(12)	−0.273(13)	
		−23.4(2)	0.083(14)	−0.640(13)	0.764(10)	4.3[1], 5.8[c]
		−9.7(4)	0.509(7)	−0.631(10)	−0.585(11)	3.4[2]
H_α(C8)	−21.9(1)	−33.7(2)	0.865(4)	−0.397(11)	−0.308(14)	
		−23.0(2)	0.026(14)	−0.577(13)	0.816(9)	5.2[1], 5.8[c]
		−9.0(4)	0.501(7)	0.714(9)	0.489(12)	0.9[3]
H_β(71)	139.8(1)	144.8(2)	0.823(10)	−0.354(22)	−0.444(18)	
		138.6(2)	0.017(33)	−0.766(35)	0.642(36)	
		136.0(2)	0.568(14)	0.536(46)	0.624(36)	
H_β(72)	113.7(1)	119.2(2)	0.862(7)	0.309(18)	−0.402(16)	
		112.2(2)	0.002(30)	0.791(32)	0.612(41)	
		109.8(2)	−0.507(12)	0.528(46)	−0.681(33)	

[a] Uncertainties are given at the 95% confidence level in the last digit(s) of the quoted values. [b] Crystallographic directions:[7]

(1) ⊥ phenyl moiety	0.1090	−0.5857	0.8028
(2) C6−HC6 bond direction	0.5289	−0.6563	−0.5381
(3) C8−HC8 bond direction	0.4919	0.7232	0.4848
(4) C7−HC7 bond direction	0.9966	0.0661	−0.0479

[c] Angle between the eigenvectors of the two intermediate α-proton coupling principal values.

fit nicely with corresponding directions calculated from the crystal structure assuming a sp^2 hybridization at C2 coplanar with the C2−N(H)−C(O) fragment, as shown in Table 1. The spin density of the carbon $2p_\pi$ orbital may be obtained from the isotropic and the anisotropic components of the hyperfine coupling tensors. The spin density from the isotropic values was obtained using the McConnell relation[13] with a *Q* value of −72 MHz,[14] whereas the spin density from the dipolar part of the coupling tensors was obtained using the method described by Gordy[15] and by Bernhard.[16] The results are presented in Table 3, together with the isotropic spin density calculated using the INDO RHF/CI semiempirical approach described by Oloff and Hüttermann.[17] Looking at the tensor data in Table 1, there clearly is a spread in the dipolar coupling of the two protons. The data in Table 3, however, suggest that this most probably is due to variations in the C−H bonding lengths and not indicative of bending at the α-carbon atom.[18]

TABLE 3: Carbon $2p_\pi$ Spin Densities Calculated from the Isotropic and Dipolar Components of the α-Proton Coupling Tensors of Radical 1, Measured at 77 K[6] and at 295 K (Table 1) as Well as the Isotropic Spin Density Calculated Using the RHF/CI INDO MO Method[a]

	77 K	295 K	RHF/CI INDO
isotropic	0.713	0.717	0.708
dipolar	0.683	0.715	

[a] All experimental values are mean values of the two tensors.

3.1.2. Nitrogen Hyperfine Coupling. The nitrogen hyperfine and quadrupolar coupling tensors in Table 1 are similar to those obtained at 77 K.[6] A more detailed picture of the electron distribution of the nitrogen 2p orbitals may be evaluated from these data. The principal values of the experimental dipolar coupling tensor of the ^{14}N coupling are (1.93, −0.49, −1.44) MHz, and the eigenvector of the largest principal value deviates

only 8.6° from the perpendicular to the sp_2-hybridized orbitals of the N atom. Similarly, the eigenvector for the intermediate principal value is close to that of the N−C_2 bond direction (deviation 17.7°). Thus, in the following a local coordinate system with the *x*-axis along the perpendicular to the C_3−N−C_2 plane and the *y*-axis along the N−C_2 bond is used as an approximation for the principal axis system for the nitrogen hyperfine coupling. The dipolar coupling from a 2p orbital with unit spin to an α-hydrogen is given by McConnell and Strathdee.[19] When the 2p orbital is located on a carbon, the coupling to an α-^{14}N atom is given by (−0.67, 2.12, −1.45) MHz with the eigenvectors to the largest eigenvalue pointing in the C2−N direction and the intermediate value in the direction of the lone pair (calculated with $Z^* = 3.18$, $R = 1.446$ Å, and the nuclear *g* factor for N, 0.4038). If the spin in the lone electron 2p orbital at C2 is assumed to be $\rho = 0.70$, it contributes a dipolar coupling tensor with principal elements (−0.47, 1.48, −1.02) MHz. This is sufficiently different from the experimental values that additional contributions to the coupling must be present. The polarization of the electron spins in the •C−N bond as well as the π conjugation of the unpaired electron must be considered as follows.

Firstly, the spin localized in the nitrogen 2p orbital participating in the σ bond to C2 will contribute to the dipolar coupling tensor. The spin density in this $2p_\sigma$ orbital is approximated as follows. From the isotropic value −8.09 MHz the nitrogen 2s spin density is obtained by scaling with the constant 1811 MHz[20] and becomes −0.00446. The s/p ratio for the nitrogen sp_2 valence orbital is obtained from standard sp_2 hybridization (see below) and gives a 2p spin density of −0.00892 for the nitrogen $2p_\sigma$ orbital of the C2−N bond. With unit spin density in a nitrogen 2p orbital the dipolar tensor is (−47.8, 95.6, −47.8) MHz[21] with the symmetry axis along the 2p orbital direction. From this a contribution of (0.43, −0.85, 0.43) MHz is expected to the dipolar tensor from the unpaired spin density of the nitrogen 2p orbital of the C2−N bond. Clearly, neglecting eventual spin density in the two other $2p_\sigma$ orbitals on N makes the total contribution due to spin polarization uncertain.

Secondly, a contribution from spin density in the lone pair orbital at the N atom due to conjugation with the lone electron orbital at the neighboring carbon atom is expected. This should give an axially symmetric tensor with the symmetry axis along the lone pair orbital direction (i.e. along the *x*-axis). The spin density in the lone pair orbital can then be estimated from the experimental value:

$$\begin{bmatrix}-0.47\\1.48\\-1.02\end{bmatrix}+\begin{bmatrix}0.43\\-0.85\\0.43\end{bmatrix}+\rho_{l.p.}\begin{bmatrix}95.6\\-47.8\\-47.8\end{bmatrix}\approx\begin{bmatrix}1.93\\-0.49\\-1.44\end{bmatrix}=\begin{bmatrix}d_x\\d_y\\d_z\end{bmatrix}$$

The three equations for $\rho_{\mathrm{l.p.}}$ yield a medium value of $\rho_{\mathrm{l.p}} = 0.021 \pm 0.04$. This gives a total theoretical dipolar tensor of (1.97, −0.38, −1.59) MHz with the eigenvalue of the positive value directed along the lone pair direction and the intermediate value directed along the C2−N direction.

3.1.3. Nitrogen Nuclear Quadrupole Interaction. The Townes/Dailey approximation[22] yields a method to estimate the nuclear quadrupolar tensor. Starting from the quadrupole operator, being a single-electron operator, the expectation values may be expressed as a sum of the expectation values for all single particle states $\psi^{(k)}$ involved,

$$Q_{ij} = \frac{-e^2Q}{4\pi\epsilon_0 2I(2I-1)h}\sum_k\left\langle\psi^{(k)}\left|\frac{3x_ix_j - r^2\delta_{ij}}{r^5}\right|\psi^{(k)}\right\rangle \quad (1)$$

where *Q* is the nuclear quadrupole moment. Within the LCAO approximation, this may be expressed as

$$Q_{ij} = \frac{-e^2Q}{4\pi\epsilon_0 2I(2I-1)h}\mathrm{Tr}(\rho\hat{Q}_{ij}) \quad (2)$$

where ρ is the density matrix and $\hat{Q}_{ij}$ is the matrix of one specific quadrupole operator, specified by the Cartesian coordinates *ij*. Townes and Dailey[22] argued that only the one-center contributions to this expression should be taken into account. For the nitrogen atom, only the $2p_x$, $2p_y$, and $2p_z$ orbitals are to be considered. Letting the indices *i*,*j* refer to the Cartesian coordinates *x*,*y*,*z*, eq 2 was evaluated by McDowell and Naito[23] and Böttcher et al.[24] Defining the four generalized orthonormal nitrogen atomic orbitals as

$$\Phi^{(k)} = a_s^{(k)}|s\rangle + a_x^{(k)}|p_x\rangle + a_y^{(k)}|p_y\rangle + a_z^{(k)}|p_z\rangle, \quad k = 1, 2, 3, 4 \quad (3)$$

the quadrupolar tensor becomes[11]

$$Q_{ij}(\mathrm{Hz}) = -\frac{e^2Q}{4\pi\epsilon_0 2I(2I-1)h}a_0\sum_k\left[\frac{3}{2}(a_i^{(k)}a_j^{(k)}) - \frac{1}{2}\delta_{ij}(a_x^{(k)^2} + a_y^{(k)^2} + a_z^{(k)^2})\right]\sigma_k \quad (4)$$

where σ_k is in the range of 0−2 and denotes the valence orbital coefficient (electron population) in the bonding molecular orbital modeling the *k*th bond (assuming a RHF model). The factor $-(e^2Q/4\pi\epsilon_0 2I(2I-1)h)a_0$ has a value between −5.0 and −4.0 MHz.[25] In this work, −4.5 MHz has been used.

The assumption of a perfect sp_2 hybridization of the nitrogen atom in hippuric acid with the lone pair in the *z*-direction and the N−H4 bond in the *x*-direction, as shown in Figure 4, gives nitrogen atomic orbitals:

$$\Phi^{\mathrm{l.p.}} = |p_z\rangle$$

$$\Phi^{\mathrm{NH4}} = (1/\sqrt{3})|s\rangle + (\sqrt{2}/\sqrt{3})|p_x\rangle$$

$$\Phi^{\mathrm{NC2}} = (1/\sqrt{3})|s\rangle - (1/\sqrt{6})|p_x\rangle - (1/\sqrt{2})|p_y\rangle \quad (5)$$

$$\Phi^{\mathrm{NC3}} = (1/\sqrt{3})|s\rangle - (1/\sqrt{6})|p_x\rangle - (1/\sqrt{2})|p_y\rangle$$

Inserting eq 5 into eq 4 yields the quadrupolar coupling tensor elements

$$Q_{xx} = (-4.5\mathrm{MHz})\left[\frac{2}{3}a - \frac{1}{12}(b+c) - \frac{1}{2}d\right]$$

$$Q_{yy} = (-4.5\mathrm{MHz})\left[-\frac{1}{3}a - \frac{5}{12}(b+c) - \frac{1}{2}d\right]$$

$$Q_{zz} = (-4.5\mathrm{MHz})\left[-\frac{1}{3}a - \frac{1}{3}(b+c) + d\right] \quad (6)$$

$$Q_{xy} = (-4.5\mathrm{MHz})\frac{\sqrt{3}}{4}(b-c)$$

$$Q_{xz} = Q_{yz} = 0$$

Here, *a* is the valence orbital population of the N−H4 bond, *b* and *c* are the orbital populations of the two N−C bonds N−C2 and N−C3, respectively, and *d* is the orbital population of the lone pair orbital.

The experimental quadrupolar tensor rotated into the same basis as the theoretical tensor of eq 6 becomes

$$\begin{bmatrix} 0.302 & -0.129 & -0.173 \\ -0.129 & 0.488 & 0.216 \\ -0.173 & 0.216 & -0.790 \end{bmatrix} \quad (7)$$

From the diagonal elements of eq 7 and the theoretical model of eq 6, the values of a and $b + c$ can be determined as a function of d. This gives $a = d - 0.15$ and $b + c = 2d - 0.38$. The Q_{xy} value gives $b - c = 0.066$, and thus $b = d - 0.16$ and $c = d - 0.22$. According to the model, the Q_{yz} and Q_{zx} should be zero. The experimental values differ from this. The model assumes a perfect sp_2 hybridization as given in Figure 4, and any inconsistency with this will make these terms differing from zero. Both bonding angles different from the ideal 120° and eventual nonplanarity at the nitrogen atom will contribute to these nonzero tensor elements.

With $d = 2$, then $a = 1.85$, $b = 1.84$, and $c = 1.78$. These values are larger than any values previously calculated[23,24,26] from quadrupolar tensors, as shown in Table 4. The reason for these large values is most probably that due to participation of the lone pair orbital on N in π bonding, the electron density d is less than 2.0. This assumption is supported by the results from our RHF/CI INDO MO calculations that yielded a d value of about 1.55. Using this value, $a = 1.41$, $b = 1.40$, and $c = 1.34$.

The result that b and c are smaller than a is understood in terms of the fact that the electron distribution in a bond depends on the electronegativity of the different atoms constituting this bond.[27] The electronegativity for N is 3.0, for C it is 2.5, and for H, 2.1.[28] As a result, the carbon atom attracts more of the bonding electrons in the C−N bond than protons in the H−N bonds do. Thus, the electron population on the nitrogen side of the bonding orbital of N to H becomes greater than in the orbitals of N to C. This confirms the sign of the quadrupolar tensor in Table 1, as established by Chacko et al.[6] and also the negative isotropic value of the nitrogen hfc. This negative sign is indeed expected, as spin polarization probably is the major mechanism establishing spin density in the nitrogen 2s orbital.

Using the SCF RHF/CI INDO MO method for calculating the electron densities of free radicals[29] the following density matrix elements $\rho_{\mu\nu}$ around the nitrogen atom was obtained:

$$\begin{array}{c} \begin{matrix} 2s & 2p_x & 2p_y & 2p_z \end{matrix} \\ \begin{pmatrix} 1.240 & 0.009 & 0.155 & -0.016 \\ & 1.189 & -0.000 & -0.007 \\ & & 1.092 & 0.040 \\ & & & 1.554 \end{pmatrix} \end{array}$$

Here, z is along the perpendicular to the C2−N−C3 fragment, and x is along the N−H bond direction. Assuming perfect sp_2 hybridization, this corresponds to the valence orbital coefficients

$$a = (1/3)\rho_{s,s} + (2/3)\rho_{x,x} = 1.206$$

$$b = c = (1/3)\rho_{s,s} + (1/6)\rho_{x,x} + (1/2)\rho_{y,y} = 1.158$$

$$d = \rho_{z,z} = 1.554$$

This method of calculating the electron density is not directly comparable to results using the Townes/Dailey approach, as two-center integrals to some extent are taken into account. This will in particular influence the absolute magnitudes of the parameters. The relative magnitudes of a and b,c compare favorably with the results obtained above using the MO-calculated $d = 1.55$ together with the experimental quadrupolar tensor elements.

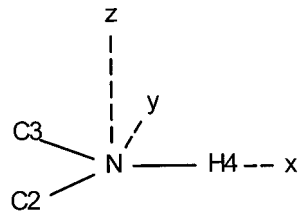

Figure 4. Geometry around the nitrogen atom in hippuric acid with the definition of the local coordinate system used for the discussion of quadrupolar couplings in radical **R1**.

TABLE 4: *a* and *b* Values Obtained from the Townes/Dailey Analysis of Nitrogen Quadrupolar Coupling Tensors in Different Systems[a]

a	*b*
1.39[24]	
1.50[24]	1.36
1.56[26]	1.43
1.53[23]	

[a] References 24 and 26 are sp_3; ref 23 is sp_2.

3.2. Radical R2. In the ENDOR spectra in Figures 2b,c, several lines were observed which from the EIE spectra were associated to a second radical species (Figure 3b). Two of the couplings of this radical exhibit unusually large β-type hyperfine splitting, whereas the other two couplings of this radical, shown in Table 2, are typical α-proton-type interactions.

The two α-proton couplings are very similar. From the isotropic values, the π-spin densities are about 0.31 (using $Q = -72$ MHz in the McConnell relation),[14] showing that a considerable delocalization of the unpaired spin density occur. The eigenvectors for the minimum principal values makes an angle close to 120°, whereas the eigenvectors for the two intermediate principal values are almost parallel. These data, together with the two large β-type interactions, are characteristic for radicals formed by net hydrogen addition to the phenyl moiety of hippuric acid. A clearly related species is the cyclohexadienyl radical,[30] and corresponding radical species were formed by hydrogen addition to naphthalene[31] and to the indole moiety of tryptophan[32] and tryptamine.[33,34] The similarity of the two couplings together with the eigenvectors for the minimum α-proton principal values suggests that the structure of radical **R2** is

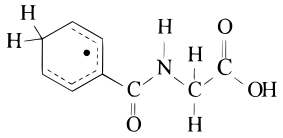

The unpaired spin density is expected to be distributed mainly within the phenyl moiety, with major spin densities at C4, C6, and C8 and with some negative spin densities at C5 and C9. The two negative spin densities should give rise to two allylic-type couplings.[33] The corresponding ENDOR lines were observed in the frequency region 15−18 MHz but could not be analyzed in detail due to overlap with more intense lines due to radical **R1**.

The sum of the two β-couplings is 253.5 MHz, which is somewhat smaller than that observed for the cyclohexadienyl radical, 267.1 MHz.[30] This is due to the slightly smaller spin densities at C6 and C8 as compared to the corresponding spin densities in cyclohexadienyl: 0.31 and 0.35, respectively. This further indicates that some of the spin is delocalized onto the carbonyl fragment in hippuric acid.

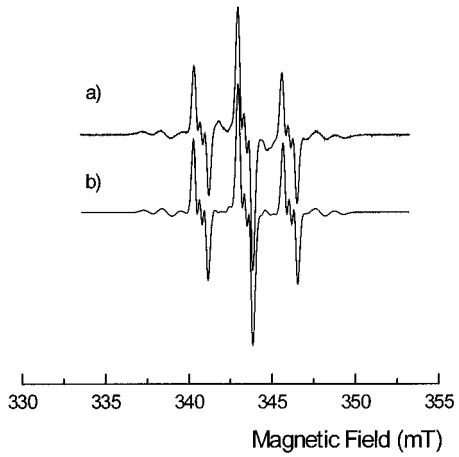

Figure 5. Experimental (a) and simulated (b) spectrum of a single crystal of hippuric acid X-irradiated at 295 K. The external magnetic field is along the crystallographic ⟨*a*⟩ axis. For the simulated spectrum the tensor data in Tables 1 and 2 were used, together with *g* values and line widths measured directly from the experimental spectra. The simulated resonances from the two radicals **R1** and **R2** were added in a proportion of 0.85:0.15

The methylene protons, if they were equivalent, would be bonded at dihedral angles close to those of the cyclohexadienyl radical, and the magnitude of the coupling is then given by[30]

$$a_{\mathrm{H}}^{\beta}(\mathrm{MHz}) = 98.1\rho_{\mathrm{eff}}$$

where the effective spin density ρ_{eff} is the composite spin density suggested by Whiffen:[35]

$$\rho_{\mathrm{eff}} = (\rho(\mathrm{C6})^{1/2} + \rho(\mathrm{C8})^{1/2})^2$$

Inserting 0.31 for the spin densities yields $\rho_{\mathrm{eff}} = 1.24$ and $\alpha_{\mathrm{H}}^{\beta} = 121.6$ MHz, close to the medium value of the two β-couplings observed (126.7 MHz). In summary, this radical is well characterized by the available experimental data.

Unfortunately, the EPR due to radical **R2** generally is masked by the much more intense resonance lines from radical **R1**. However, at most orientations broad features due to radical **R2** extend beyond the dominant resonance of radical **R1**. This is sufficient for a final test of the ENDOR spectrum interpretation by spectrum simulation routines.

3.3. Spectral Simulations. The EPR spectra due to radicals **R1** and **R2** could be well simulated using the experimental data given in Tables 1 and 2. One example of such a simulation is shown in Figure 5. The relative yields of the two radical species were adjusted for optimum fit. From a series of simulations, radical **R1** contributes about 85% of the total resonance, while radical **R2** contributes the remaining 15%.

4. Mechanistic Aspects

The basic concepts of the radiation chemistry of amino acids are fairly well-known after the pioneering studies in the 1960s.[3,4,36] Both the primary oxidation and reduction products are localized at the carboxylic moiety of the molecule. The oxidation product is very unstable and rapidly decomposes by decarboxylation. The subsequent product then usually becomes involved in intermolecular reactions, leading to a variety of secondary radicals observable at room temperature. The reduction product is more stable, but ultimately decomposes by deamination. This deamination product very often is stable at room temperature.

This basic (and indeed simplified[4]) scheme of processes is modified when amino acids with more complex side groups are studied. This is, in particular, the case for the sulfur-containing and aromatic side groups. Several studies also have been made using various amino acids analogues showing that although the concepts outlined above still basically are valid, modifications are introduced depending upon the electronic and geometrical properties of the substituent groups.[9,11]

Only a few dipeptides have so far been studied in any detail in the crystalline state by EPR and ENDOR spectroscopy.[4,37] In short, whereas the oxidative processes in dipeptides seem to be similar to those in the simple amino acids, reduction products now appear both at the carboxyl group and at the peptide linkage (carbonyl oxygen), and subsequent reactions (deamination, C−N bond scission) originate from both these positions.

The room-temperature products observed in hippuric acid may be compared to processes taking place in the dipeptide systems. In the following, possible mechanisms leading to the observed products are suggested. However, detailed low-temperature studies are required to establish the actual reactions occurring.

After the primary ionization event, the carboxyl cation is formed. In analogy with the reactions in amino acids and dipeptides, this product is suggested to deprotonate, followed by decarboxylation leading to radical **R1**:

$$\mathrm{Ph{-}CO{-}NH{-}CH_2{-}COOH} - \mathrm{e^-} \rightarrow$$
$$(\mathrm{Ph{-}CO{-}NH{-}CH_2{-}COOH})^+ \rightarrow$$
$$(\mathrm{H^+}) + \mathrm{Ph{-}CO{-}NH{-}{}^{\bullet}CH_2} + \mathrm{CO_2}$$
$$\textbf{R1}$$

As also noted by Chacko et al.,[6] it is interesting that the generally very unstable decarboxylation product is stable at room temperature. This may be ascribed to resonance stabilization of **R1** due to delocalization of the unpaired electron density onto the carbonyl moiety and the phenyl ring.

In the aliphatic dipeptides, the primary ejected electrons may be captured both at the carboxy group (I) and in the peptide carbonyl group (II):

$$2(\mathrm{R{-}CO{-}NH{-}CH_2{-}COOH} + \mathrm{e^-}) \rightarrow$$
$$\mathrm{R{-}CO^{\bullet -}{-}NH{-}CH_2{-}COOH\ (I)} +$$
$$(\mathrm{R{-}CO{-}NH{-}CH_2{-}COOH})^{\bullet -}\ \mathrm{(II)}$$

C−N bond rupture ("deamination") may then take place on either side of the nitrogen. In the present work, no products that may be ascribed to deamination-type products were observed. On the contrary, in the aromatic amino acids, deamination radicals usually are observed together with products formed by net hydrogen addition to the aromatic moiety.[32,38,39]

As judged from the room-temperature data of hippuric acid, it seems as if the aromatic phenyl group of hippuric acid protects the peptide bond from reductive bond cleavage. Apparently, the processes involving the reduction pathway become localized at the aromatic substituent. Possibly, the phenyl moiety scavenges electrons, and radical **R2** is formed by protonation of the aromatic anion radical. However, only detailed low-temperature studies can distinguish this mechanism from the alternative of hydrogen addition to the phenyl moiety. Hydrogen atoms may be produced by decomposition of carboxyl anions by mechanisms other than deamination.

Acknowledgment. Two of the authors (N.A.S., O.I.E.) are grateful for the financial support from ISSP, Uppsala, Sweden, and Prof. Lennart Hasselgren. Enlightening discussions with Mr.

Anders Sørnes, Department of Physics, University of Oslo, are acknowledged.

References and Notes

(1) Poole, C. P., Farach, H. C., Eds. *Handbook of Electron Spin Resonance*; American Institute of Physics Press: New York, 1994.
(2) Close, D. M. *Magn. Reson. Rev.* **1988**, *14*, 1, and references therein.
(3) Iwasaki, M. *MTP International Review of Science; Physical Chemistry Series One*; Butterworth University Park Press: New York, 1972; Vol 4, p 317.
(4) Box, H. C. *Radiation Effects. ESR and ENDOR Analysis*; Academic Press: New York, 1977.
(5) Votinov, M. P. *Radiobiologiya* **1961**, *1*, 149.
(6) Chacko, V. P.; McDowell, C. A.; Singh, B. C. *J. Chem. Phys.* **1980**, *72*, 4111.
(7) Currie, M.; MacDonald, A. L. *J. Chem. Soc., Perkin Trans. 2* **1974**, 784.
(8) Hole, E. O.; Sagstuen, E. *Radiat. Res*. **1987**, *109*, 190.
(9) Sanderud, A.; Sagstuen, E. *J. Phys. Chem*. **1996**, *100*, 9545.
(10) Claesson, O.; Lund, A.; Jørgensen, J. P.; Sagstuen, E. *J. Magn. Reson*. **1980**, *41*, 229.
(11) Sørnes, A. R.; Sagstuen, E.; Lund, A. *J. Phys. Chem*. **1995**, *99*, 16867.
(12) Sagstuen, E.; Hole, E. O.; Haugedal, S. R.; Lund, A.; Eid, O. I.; Erickson, R. *Nukleonika*, in press.
(13) McConnell, H. M.; Chesnut, D. B. *J. Chem. Phys.* **1958**, *28*, 107.
(14) Bernhard, W. A. *Adv. Radiat. Biol.* **1981**, *9*, 199.
(15) Gordy, W. *Theory and Applications of Electron Spin Resonance*; John Wiley & Sons: New York, 1980.
(16) Bernhard, W. A. *J. Chem. Phys*. **1984**, *81*, 5928.
(17) Oloff, H.; Hüttermann, J. *J. Magn. Reson*. **1980**, *40*, 414.
(18) Sørnes, A. R.; Sagstuen, E. *J. Phys. Chem*. **1995**, *99*, 16857.
(19) McConnell, H. M.; Strathdee, J. *Mol. Phys.* **1959**, *2*, 129.
(20) Morton, J. R.; Preston, K. F. *J. Magn. Reson*. **1978**, *30*, 577.
(21) Morton, J. R.; Rowlands, J. R.; Whiffen, D. H. *Atomic Properties for Interpreting ESR Data*; National Physics Laboratory: BPR 13, 1962.
(22) Townes, C. H.; Dailey, B. P. *J. Chem. Phys.* **1949**, *17*, 782.
(23) McDowell, C. A.; Naito, A. *J. Magn. Reson*. **1981**, *45*, 205.
(24) Böttcher, R.; Metz, H.; Windsch, W. *J. Chem. Phys*. **1985**, *93*, 137.
(25) Schweiger, A. *Struct. Bond.* **1982**, 51.
(26) Pöppl, A.; Völkel, G. *Chem. Phys.* **1993**, *171*, 387.
(27) Morton, J. R.; Preston, K. F. *J. Magn. Reson*. **1978**, *30*, 577.
(28) Atkins, P. W. *General Chemistry (Int. Student Edition)*; Scientific American Books, W. H. Freeman & Co: New York, 1989.
(29) Pople, J. A.; Beveridge, D. L. *Approximate Molecular Orbital Theory*; McGraw-Hill: New York, 1970.
(30) Fessenden, R. W.; Schuler, R. H. *J. Chem. Phys*. **1963**, *38*, 773.
(31) Böhme, U. R.; Wolf, H. C. *Chem. Phys. Lett*. **1972**, *17*, 582
(32) Sagstuen, E.; Byrkjeland, H. G.; Henriksen, T. *Radiat. Res*. **1978**, *74*, 10.
(33) Theisen, H.; Sagstuen E. *J. Chem. Phys.* **1981**, *74*, 2319.
(34) Theisen, H.; Sagstuen E. *J. Chem. Phys.* **1983**, *78*, 2254.
(35) Whiffen, D. H. *Mol. Phys*. **1963**, *6*, 233.
(36) Henriksen, T.; Saxebøl, G.; Melø, T. B. In *Free radicals in Biology*; Pryor, W. A., Ed.; Academic Press: New York, 1976; Vol. 2, p 213.
(37) Helms, H. A.; Suzuki, I.; Miyagawa, M. *J. Chem. Phys*. **1973**, *59*, 5055.
(38) Westhof, E.; Flossmann, W.; Müller, A. *Int. J. Radiat. Biol*. **1975**, *27*, 51.
(39) Flossmann, W.; Westhof, E. *Int. J. Radiat. Biol*. **1978**, *33*, 139.